Characterization of the Reaction Mechanism for *Trypanosoma brucei* Ornithine Decarboxylase by Multiwavelength Stopped-Flow Spectroscopy†

Harold B. Brooks and Margaret A. Phillips*

Department of Pharmacology, University of Texas Southwestern Medical Center, 5323 Harry Hines Boulevard, Dallas, Texas 75235-9041

Received July 9, 1997; Revised Manuscript Received September 19, 1997⊗

ABSTRACT: Ornithine decarboxylase (ODC), a pyridoxal 5′-phosphate (PLP)-dependent enzyme, catalyzes the first committed step in the biosynthesis of polyamines. The UV−visible spectra of PLP (300−500 nm) was used to monitor the formation and breakdown of ODC reaction intermediates by multiwavelength stopped-flow spectroscopy to determine the reaction mechanism. Global kinetic analysis of the spectral data acquired after mixing ODC with saturating substrate (S) or product (P) (10 mM ornithine or 10 mM putrescine at 4 °C) suggests that ODC-catalyzed decarboxylation proceeds by the following reaction mechanism: ODC + S ⇔ A → B → C → D → E/F ⇔ ODC + P, where A−F are intermediates along the reaction path. Species B, which has absorbance maxima of 350 and 450 nm, is spectrally distinct from the other intermediates. On the basis of the calculated spectral characteristics, species B is likely to represent a quinoid intermediate which would be formed directly upon decarboxylation of ornithine. Thus, the data suggest that the reaction proceeds via formation of a Schiff base intermediate (species A) during the dead time of the stopped-flow instrument, followed by formation of a quinoid intermediate with a rate constant of 21 s^{-1}. The quinoid intermediate decays in two steps (with rates of 145 and 1.0 s^{-1}, respectively) to a Schiff base with putrescine (species D). Protonation of the C_α carbon is required for the formation of species D, suggesting that the first of these events represents this step. The decay of species D to free enzyme and product occurs via a minimum of two intermediates and at an overall rate constant of 1−3 s^{-1}. By comparison to the steady-state turnover number (k_{cat} = 0.5 s^{-1} at 4 °C), these data identify product release as a rate-determining step in the overall reaction.

Ornithine decarboxylase (ODC), a pyridoxal 5′-phosphate (PLP)-dependent enzyme, catalyses the decarboxylation of Orn to putrescine in the first step of polyamine biosynthesis (*1*).[1] Polyamines are required for cellular proliferation, ODC is under cell cycle control, and not surprisingly increased ODC activity has been linked to neoplasm (*2*). ODC is a proven pharmacological target: α-difluoromethylornithine (DFMO), a suicide inhibitor of ODC, is used to treat African sleeping sickness caused by *Trypanosoma brucei* (*3*) and further has shown some efficacy against *Pneumocystis carinii* pneumonia in AIDS patients and for the treatment and prevention of some cancers (*2, 4*).

ODC is a homodimer in which the two identical active sites are formed at the dimer interface by residues from the N-terminal domain of one subunit and the C-terminal domain of the other (*5*−*7*). The PLP-binding site is primarily located in the N-terminal domain, which is predicted to fold into a β/α barrel with structural similarity to alanine racemase (*8*). The recent solution structure of alanine racemase confirms that alanine racemase folds into a β/α barrel with the PLP-binding site contained in the center of the barrel (*9*). Several important interactions in the PLP-binding site of ODC have been biochemically identified: K69 forms a Schiff base with PLP (*10, 11*); E274 stabilizes the positive charge on the pyridine nitrogen of PLP, enhancing the electron-withdrawing ability of the ring (*12*); and R277 is required for high-affinity PLP binding through interaction with the 5′-phosphate of the cofactor (*13*).

Despite the large amount of experimental effort put into understanding the function of ODC, no analysis of the reaction intermediates has been undertaken. The sensitivity of the PLP spectra to both the tautomeric and ionic states of the ring has allowed the reactions of many PLP-dependent enzymes to be monitored by either single-wavelength or multiwavelength stopped-flow spectroscopy to obtain mechanistic information. Based upon studies on other PLP-dependent enzymes, two plausible mechanisms for ODC can be drawn (Figure 1). In either mechanism the first step is expected to be formation of the external aldimine (Schiff base) with Orn. Decarboxylation could then occur either by the formation of a quinoid intermediate, as proposed for glutamate decarboxylase (*14*) and the β-subunit of tryptophan synthase (*15*), or by the formation of a butaldimine intermediate, if decarboxylation is concerted with protonation at the C4′ of PLP. The latter mechanism is based on studies of aspartate aminotransferase, in which double-isotope fractionation experiments demonstrated that a ketimine intermediate is generated directly by a concerted 1,3-prototropic shift of the C_α proton to the C4′ (*16*−*18*). However, for glutamate decarboxylase (*14*) and methionine decarboxylase (*19*), this mechanism has been proposed to operate only as a side reaction which leads to abortive transamination. The final step in product formation for either

† This work was supported by grants from the National Institute of Health (R01 AI34432), the Welch Foundation (I-1257), the American Heart Association to M.A.P., and the National Institute of Health (F32 AI09495) to H.B.B.

* Corresponding author: phone (214) 648-3637; fax (214) 648-2971.

⊗ Abstract published in *Advance ACS Abstracts,* November 15, 1997.

[1] Abbreviations: ornithine decarboxylase, ODC; pyridoxal 5′-phosphate, PLP; dithiothreitol, DTT.

S0006-2960(97)01652-8 CCC: $14.00

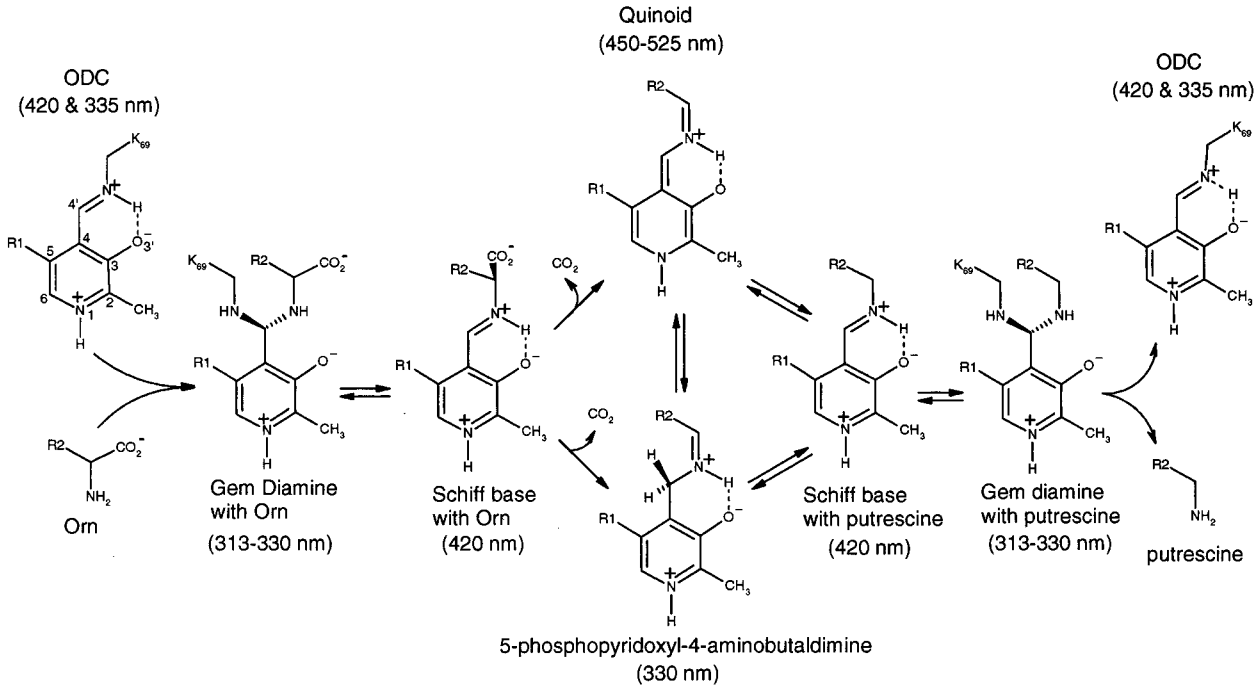

FIGURE 1: Hypothetical mechanisms for the ODC-catalyzed conversion of Orn to putrescine. R1 is $CH_2OPO_3^{2-}$ and R2 is $(CH_2)_3NH_3^+$. The wavelengths shown in parentheses are the absorbance maxima for each species. Two wavelength maxima are given for the ketoenamine (420 nm) and enolimine (335 nm) forms of the internal aldimine of ODC (*13*); however, only the ketoenamine form is shown for simplicity. For all other chemical species only the predominant spectral maximum and its tautomeric assignment are shown. The spectral maxima for these species were compiled from data reported for aspartate aminotransferase (*16*, *17*, *42*), glutamate decarboxylase (*14*), tryptophan synthase (*43*, *47*, *48*), and model compounds (*49*, *50*).

mechanism would be protonation at C_α to form putrescine, followed by transimination to generate free ODC and product.

In this paper, we report the characterization of the reaction mechanism for ODC based upon multiwavelength stopped-flow analysis over the spectral range of 300−500 nm. For the reaction of ODC with Orn, four intermediates are observed, including a species with quinoid-like characteristics which is not observed in the reaction with product. Formation of the quinoid species upon decarboxylation is not the rate-limiting step, and instead, product release is at least partially rate limiting.

MATERIALS AND METHODS

Materials. Monobasic and dibasic sodium phosphate were purchased from Fisher. Reduced glutathione was purchased from Amaresco. L-Orn, putrescine, and DTT were purchased from Aldrich. The CO_2 detection kit was purchased from Sigma.

Purification of T. brucei ODC. ODC was expressed from the cloned gene (*20*, *21*) in BL21/DE3 cells from the T7 promoter as described (*5*). The protein yield, was increased by growing cells in a New Brunswick BioFlo 3000 fermentor (10 L) in ECPM1 media (*22*). The pH was maintained at 7.2 with 85% phosphoric acid and 30% ammonium hydroxide, and the media was oxygenated to atmospheric O_2 levels. After 15 h at 30 °C, the cells reached an O.D. of 16 and were induced at 23 °C with IPTG (1.2 g) for 6 h. Cells were harvested by centrifugation, and the cell paste (700 g) was resuspended in 700 mL of lysis buffer (0.2 M NaCl, 50 mM Hepes·NaOH, 5% glycerol, 7 mM β-mercaptoethanol, 0.2 mM PLP, 2 mM PMSF, 2 μg/mL leupeptin, 4 μg/mL antipain, 20 μg/mL benzamidine, 2 μg/mL pepstatin, and 2 μg/mL chymostatin) using a Waring blender at high speed for 1 min, incubated on ice for 60 min with lysozyme (1.2 g), and lysed by sonication. ODC was purified by Ni^{2+}-agarose column chromatography as previously described (*5*). Purified ODC was equilibrated into 20 mM sodium phosphate, pH 7.3, 2 mM reduced glutathione and concentrated by ultrafiltration (Amicon YM-10). Stock protein solutions (1−2 mM) were stored at −80 °C. Typical yields were 2 g of purified ODC as determined from the absorbance at 280 nm (*5*).

Steady-State Kinetics. Steady-state kinetics of ODC (0.25−5.0 μM) and Orn (0.04−10 mM) at 4 and 25 °C were obtained in 10 mM sodium phosphate pH 7.3 by directly monitoring the loss in chirality of Orn upon decarboxylation by circular dichroism (*23*). The rates were fit to the Michaelis−Menten equation to obtain the steady-state parameters (at 4 °C, $k_{cat} = 0.51 \pm 0.03$ s^1 and $K_m = 96 \pm 30$ μM). The parameters for ODC at 37 °C have been previously reported ($k_{cat} = 13.2 \pm 1.6$ s^{-1} and $K_m = 620 \pm 170$ μM (*23*)).

The inhibition kinetics for DTT on the reaction of ODC and Orn were determined using the standard NADH-linked assay at 37 °C (*5*). The rates were fit to the equation for a competitive inhibitor (*24*).

Pre-Steady-State Kinetics Data Collection. The pre-steady-state kinetics of ODC with Orn and putrescine were monitored using a Biologic SFM3 mixer equipped with a TC-100 quartz cell (path length of 1 cm) coupled to a J&M Tidas16 512 diode array for multiwavelength data collection (Molecular Kinetics, Pullman, WA) or to an Aviv 62DS circular dichroism spectrometer for single-wavelength data collection. The SFM3 using the TC-100 cell has a dead time of 3 ms with a flow velocity of 12 mL/s. The diode array has a spectral acquisition time of 1.3 ms at a wavelength resolution of 0.84 nm over a range of 197−620 nm.

To monitor the reaction of Orn (0.2−10 mM) or putrescine (0.2−10 mM) with ODC (0.16 mM), the mixer was set up with three 21 mL syringes containing buffer (20 mM sodium phosphate pH 7.3), substrate (Orn or putrescine), and ODC (0.3 mM), respectively. Buffer was mixed with substrate to yield 2 times the desired substrate concentration (total volume 0.15 mL) in mixer 1. The contents were then mixed with ODC (0.15 mL), and monitoring of the reaction was initiated. Multiwavelength data were collected from 197 to 620 nm over two different time regimes, 3−300 and 20−5000 ms. A total of 256 spectra were collected for each multiwavelength data set. Single-wavelength data were collected at 420 and 340 nm over three time regimes: 3−50, 3−500, and 3−5000 ms; 1000 data points were collected for each data set. All experiments were repeated 2−3 times for each of the time regimes, thus, at a given concentration of reactants the reaction was observed 4−9 times.

For the measurement of putrescine off rates, buffer was loaded into syringe 1 (21 mL), ODC (0.3 mM) premixed with putrescine (4 mM) was loaded into the syringe 2 (5 mL), and DTT (0.2−0.4 nM) was loaded into the third syringe (21 mL). Buffer (0.12 mL) was mixed with ODC−putrescine (0.03 mL), and the contents were then mixed with DTT (0.15 mL). The reaction was monitored at 420 nm.

Pre-Steady-State Kinetics, Data Analysis. Analysis of Single-Wavelength Data. Single-wavelength data were fit using Biokine software (Biologic, France) to eq 1, where A

$$A = \sum_{i=1}^{n} A_i \exp(-k_{\mathrm{obs}i}t) + b \qquad (1)$$

is the measured absorbance, $k_{\mathrm{obs}i}$ are the observed rate constants, t is time, b is an offset to represent a nonzero baseline, and A_i are the amplitudes associated with $k_{\mathrm{obs}i}$.

Global Kinetic Analysis of Pre-Steady-State Reactions. Multiwavelength data were fit using Specfit 2.10 (Spectrum Software Associates, Chapel Hill, NC), which uses singular value decomposition (SVD analysis) to solve for the spectral eigenvectors (*25*). The eigenvectors were then used to reconstruct the spectra of chemical species and their kinetics using a model-dependent multivariate least-squares implementation of the Levenberg−Marquardt algorithm (*26*). Data from selected wavelengths (340, 420, and 450 nm) were first fit to eq 1 to provide initial estimates of the rate constants for the Specfit global data analysis. Numerous models were examined, and the quality of the fits was evaluated by the standard deviation (σ) of the observed absorbance and by analysis of residual plots. The data for the slow phases was analyzed first (20−5000 ms data). The results of these fits were used to constrain the rate constant for the slow process when analyzing the fast time regime data analyzed (3−300 ms).

Pre-Steady-State Analysis of the Reaction of DTT with ODC. DTT binds to the active site of ODC in the absence of substrate or product and alters the spectra of enzyme-bound PLP causing a decrease in absorbance at 420 nm. The reaction of DTT with free ODC was monitored at both 4 and 25 °C and the data fit to a single exponential (eq 1) to obtain k_{obs}. The concentration dependence of k_{obs} on DTT was determined by fitting the data to eq 2 (*27*, *28*) using Sigma Plot for Mac (Jandel Scientific), where k_{on} is the association rate constant and k_{off} is the dissociation rate constant.

$$\mathrm{ODC} + \mathrm{DTT} \underset{k_{\mathrm{off}}}{\overset{k_{\mathrm{on}}}{\rightleftharpoons}} \mathrm{ODC{\cdot}DTT} \qquad k_{\mathrm{obs}} = k_{\mathrm{on}}[\mathrm{DTT}] + k_{\mathrm{off}} \qquad (2)$$

Spectral Deconvolution of Pre-Steady-State Intermediates. Spectra acquired at different time points along the reaction of ODC with Orn were analyzed to determine the identity of individual bands contributing to the overall spectra utilizing a log-normal equation (eq 3)

$$\epsilon(\nu) = \sum_{i=1}^{n} \epsilon_i \exp\left(-\ln 2 \frac{\ln^2\left(1 + \dfrac{(\nu - \nu_i)(\rho_i^2 - 1)}{\omega_i \rho_i}\right)}{\ln^2 \rho_i}\right) \qquad (3)$$

where

$$\epsilon_i = \frac{A_i \exp(-c^2/2)}{\omega_i \sqrt{2\pi} \dfrac{\rho_i}{\rho_i^2 - 1} c} \quad \text{and} \quad c = \frac{\ln \rho_i}{\sqrt{2 \ln 2}}$$

as previously described (*29*−*35*). The parameters of eq 3 are defined as follows: $\epsilon(\nu)$ is the extinction coefficient of ODC at wavenumber ν, ϵ_i is the apparent extinction coefficient at the wavenumber of maximal absorbance (ν_i), for any given band i of width, ω_i, skewness, ρ_i and area, A_i.

The data were fit to eq 3 using Peakfit (SPSS, Chicago IL) through an iterative process where first the two Schiff base tautomers were included and additional species, notably the quinoid tautomers, were added until a good fit was obtained. The parameters defining each species were calculated from eq 3 by providing initial estimates obtained from the literature for the Schiff base and quinoid species (*32*−*34*). All parameters were allowed to float during the final calculations. The fraction of each species contributing to the observed spectra was then calculated by comparing the area (A_i) under each curve to the molar area (A_o) for a 1 M solution of a pure species. The A_o's for the 445, 420, and 328 nm bands were obtained from the literature as follows: A_o for the 445 nm band was assumed to be the same as observed for the quinoid of tryptophanase (*35*), while the A_o's for the 420 and 328 nm bands of ODC were calculated based on the ketoenamine and enolimine for the Schiff bases reported for aspartate aminotransferase and tryptophanase (*33*, *35*). A_o for the 360 nm band was obtained by normalizing the A for the 360 nm band to the remaining unaccounted fraction of ODC.

Molecular Orbital Calculations. AM1 wave function calculations (*36*) were performed using Spartan v 4.0.3 (Wavefunction Inc., Irvine CA) to calculate the heats of formation for the addition of a proton to the two quinoid tautomers at C4′ or C_α.

RESULTS

Effect of DTT on the Pre-Steady-State Kinetics. ODC-bound PLP has two spectral maxima at 335 and 420 nm (Figure 2). These bands arise from the two tautomers of the Schiff base formed to K69 (internal aldimine) in the active site (*13*). Addition of DTT, which is traditionally included during purification and assay of ODC to stabilize the enzyme, causes a loss of the 420 nm absorbance maximum and an increase in the 335 nm peak (Figure 2). Thiols have previously been reported to react with PLP to form adducts which have a characteristic absorbance at 330

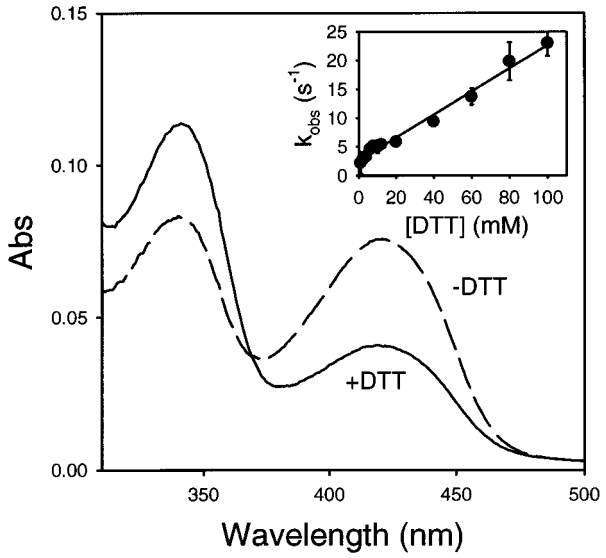

FIGURE 2: Analysis of the reaction of ODC with DTT. The dashed line is the spectrum of ODC (0.03 mM) in 20 mM phosphate, pH 7.3. The solid line is the spectrum of ODC (0.03 mM) after addition of 2 mM DTT. The inset shows the rate constants (k_{obs}) for formation of DTT−ODC as measured by stopped flow at 420 nm. The solid line is a fit to eq 2, where $k_{on} = 203 \pm 7$ M^{-1} s^{-1} and $k_{off} = 2.6 \pm 0.3$ s^{-1}. The reported errors are the standard error to the fit. All data were collected at 25 °C.

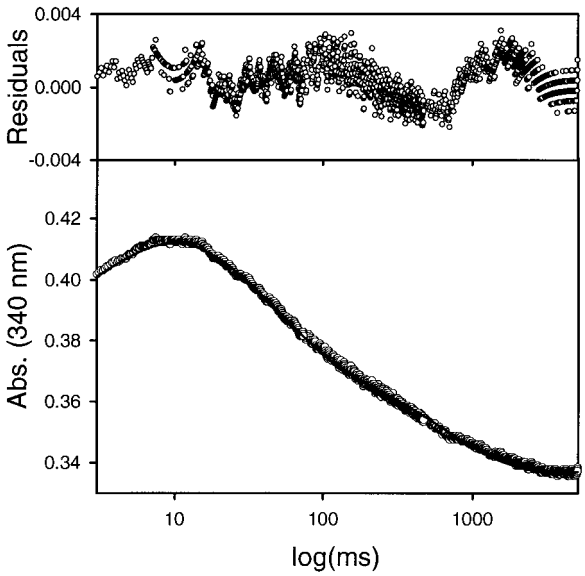

FIGURE 3: Single-wavelength analysis of the pre-steady-state reaction of Orn with ODC. The absorbance change at 340 nm (open circles) which occurs upon mixing Orn (10 mM) and ODC (0.16 mM) is plotted vs log(time in ms). The data were best fit to the three exponential form of eq 1 (solid line), where, $A_1 = -0.0453 \pm 0.0003$, $A_2 = 0.0503 \pm 0.0002$, $A_3 = 0.0359 \pm 0.0001$, $k_{obs1} = 306 \pm 4$ s^{-1}, $k_{obs2} = 18.6 \pm 0.1$ s^{-1}, $k_{obs3} = 1.48 \pm 0.01$ s^{-1}, and $b = 0.33730 \pm 0.00004$. The reported errors are the standard error to the fit. The residuals to this fit are shown in the top panel.

nm (*37*). The absorbance change at 420 nm can be fit to a single-exponential decay (eq 1). The observed rate constant (k_{obs}) is linearly dependent upon DTT concentration (Figure 2, inset) and the data were fit to eq 2 to obtain the rate constants for the binding of DTT to ODC ($k_{on} = 203 \pm 7$ M^{-1} s^{-1}, $k_{off} = 2.6 \pm 0.3$ s^{-1}, and $K_d = 13 \pm 2$ mM at 25 °C). The DTT off rate is slow compared to the k_{cat} (6.2 ± 0.4 s^{-1}) determined for the steady-state reaction of Orn with ODC under these conditions. Thus, in the pre-steady-state reaction of DTT−ODC with Orn or putrescine, the DTT off rate dominates the observed spectral changes and substrate-dependent spectral changes cannot be observed. Consequently, DTT was excluded from all remaining spectral studies except where noted, and reduced glutathione, which does not effect the spectral properties of ODC, was utilized to stabilize ODC during purification.

These data suggested that DTT is a competitive inhibitor of Orn. This finding was confirmed by steady-state analysis; DTT has a K_I of 9 ± 1 mM vs Orn at 37 °C. Thus, under the typically utilized steady-state assay conditions (*5*, *23*, *38*), the effect of DTT on the steady-state kinetic parameters is limited to a mild increase in the K_m for Orn (∼16% for 2 mM DTT) with no effect on k_{cat}.

Pre-Steady-State Kinetic Analysis by Single-Wavelength Stopped-Flow Spectroscopy. Single-wavelength data were collected at the spectral maxima (340 and 420 nm) for the internal aldimine of PLP bound to ODC at multiple Orn concentrations (0.2−10 mM) to obtain an estimate of the observed rate constants and to determine the substrate concentration that yielded maximum rates prior to initiating multiwavelength analysis. Initial spectra were acquired at 25 °C; however, a substantial portion of the reaction occurred during the mixing dead time under these conditions (data not shown). Subsequent data were all collected at 4 °C, where the bulk of the reaction was kinetically accessible. The data collected at 340 nm require three exponentials to obtain a fit to eq 1 (Figure 3). The spectral changes associated with k_{obs1} are substrate dependent, and maximal rates are observed for all substrate concentrations above 2 mM. In contrast, k_{obs2} and k_{obs3} are not substrate dependent, consistent with the presence of an irreversible step (data not shown). The analysis of the 420 nm data provided no additional information and is not shown. As a control, the reaction rate of solution PLP with Orn was measured under the same conditions and found to be 70-fold slower ($k_{obs} = 0.021 \pm 0.004$ s^{-1} at 10 mM Orn) than the slowest step (k_{obs3}) of the enzyme-catalyzed reaction; therefore, any excess PLP present in the enzyme prepartion does not interfere with observation of the spectral changes occurring for PLP bound to ODC.

Pre-Steady-State Kinetic Analysis of the Reaction of Orn with ODC by Multiwavelength Stopped-Flow Spectroscopy. The reaction of ODC with Orn was characterized by multiwavelength stopped-flow spectroscopy. A series of representative spectra acquired over the time course of the reaction of ODC (0.16 mM) with a saturating concentration of Orn (10 mM) at 4 °C are displayed in Figure 4a. Four distinct phases are observed for this reaction. During the dead time of the mixer, a change in the spectra of ODC occurs which is characterized by a decrease in absorbance and a red shift of the 420 nm band and by the appearance of a shoulder at 450 nm. The initial observed phase is complete within 18 ms and is characterized by an increase and a red shift in absorbance of the 335 nm band. The next kinetic phase is complete after ∼150 ms and is characterized by a general decrease in absorbance at 335, 420, and 450 nm with a blue shift of the 335 nm band. The final phase of the reaction of Orn with ODC is characterized by a decrease in absorbance at 335 nm and an increase in absorbance at 420 nm. Steady state is reached after ∼3 s. Single-wavelength analysis of these data at either 335 or 420 nm gives results

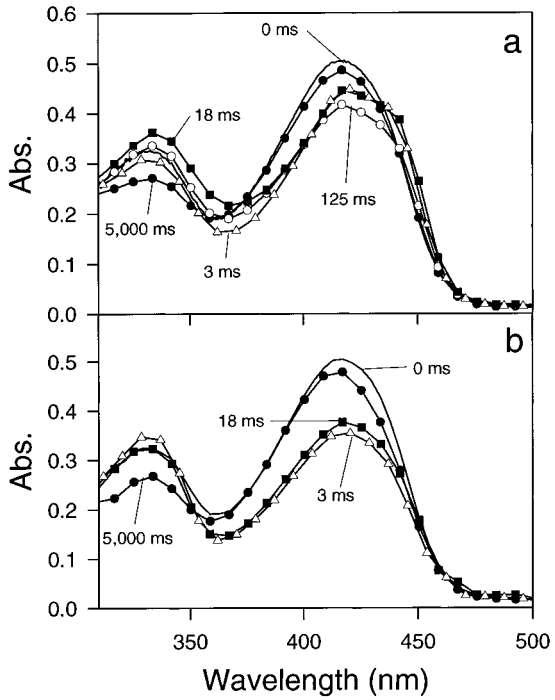

FIGURE 4: Multiwavelength stopped-flow analysis of the reactions of Orn and putresine with ODC. (a) Representative absorbance spectra of ODC (0.16 mM) at selected time points after mixing with Orn (10 mM) at 4 °C: solid line, spectra of ODC prior to additon of Orn; (△) spectra 3 ms after mixing ODC and Orn (dead time); (■) spectra 18 ms after mixing ODC and Orn; (○) spectra 125 ms after mixing ODC and Orn; (●) spectra 5000 ms after mixing ODC and Orn. (b) Representative absorbance spectra of ODC (0.16 mM) at selected time points after mixing with putrescine (10 mM) at 4 °C: solid line, spectra of ODC prior to addtion of putrescine; (△) spectra at 3 ms (dead time); (■) spectra at 18 ms; (●) spectra at 5000 ms after mixing ODC and putrescine. Data points were collected at 0.84 nm intervals, but for clarity, data points are only displayed at 7.5 nm intervals.

Scheme 1

$$A \xrightarrow{k_1} B \xrightarrow{k_2} C \xrightarrow{k_3} D$$

similar to those obtained from the single-wavelength data (above).

Global Kinetic Analysis of the Multiwavelength Data Collected for the Reaction of ODC with Orn. Global kinetic analysis of the multiwavelength data (300−500 nm) collected at saturating Orn (10 mM) was performed to determine the appropriate mechanism for the reaction, to assign rate constants, and to deconvolute the spectra of the intermediate species. The simplest model that gives a good fit to the data is a three-step sequential reaction, where A is the initial adduct formed between ODC and Orn, and B−D are intermediates interconverted by three rate constants defined during the fit such that $k_2 > k_1 > k_3$ (Scheme 1). Based on this model, the rate constants for these three steps (k_1, k_2, k_3) are calculated to be 21.1 ± 0.4, 145 ± 5, and 1.03 ± 0.01 s^{-1}, respectively. The model-derived spectra for intermediates A−D are displayed in Figure 5a and the calculated time dependencies of their concentrations are displayed in Figure 5b. No bias in the residual plots is observed over the entire wavelength range (Figure 5b) and the standard deviation of the absorbance (σ) is 0.0007 ± 0.0001. Further, the appearance of the 450 nm shoulder in the spectra after mixing with Orn most likely arises from

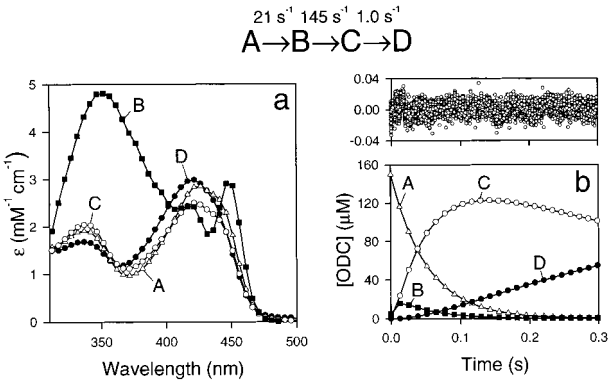

FIGURE 5: Global kinetic analysis of the multiwavelength stopped-flow data acquired after mixing ODC (0.16 mM) with 10 mM Orn (representative spectra are displayed in Figure 4a). Data were fit by global kinetic analysis to the equation describing a three-step sequential reaction model (Scheme 1), where four species (A−D) are interconverted by three rate constants (21.1 ± 0.4, 145 ± 5, 1.03 ± 0.01 s^{-1}). The standard deivation (σ) of the absorbance for this model is 0.0007 ± 0.0001. The rate constants and σ represent the average of four independent experiments; the error is the standard deviation. The analysis for a representative data set is displayed. (a) The model-derived wavelength dependence of the extinction coefficients for intermediates A (△), B (■), C (○), and D (●). (b) The model-derived concentration profiles for intermediates A−D. The residuals to the fit of the data displayed in panels a and b are shown above panel b as ϵ (mM^{-1} cm^{-1}) vs time; residuals are dislayed for data between 310 and 500 nm at 5 nm intervals. Data points were collected at 0.84 nm intervals but are displayed at 5 nm intervals.

the formation of unique spectral species during the course of the reaction. This intermediate should be predicted by correct modeling of the data, and indeed, a unique species (species B) is predicted by modeling the data to Scheme 1. The absorbance spectra of species A, C, and D have wavelength maxima at 335 and 420 nm, similar to that observed for the internal aldimine; however, species B has absorbance maxima at 350 and 450 nm, consistent with the appearance of the 450 nm shoulder. Further evidence in support of this unique spectral species comes from independent analysis of the data using log-normal distribution curves (below).

Spectral Deconvolution of the Reaction of ODC with Orn. The spectrum of ODC after mixing with Orn (10 mM) was resolved into individual absorption bands with log-normal distribution curves for five representative times along the reaction course (0, 3, 18, 125, and 5000 ms). For the time points at the beginning (0 ms) and end (5000 ms) of the reaction, the presence of only two bands arising from the two tautomers of a Schiff base species is required to obtain a good fit to the measured spectral data using eq 3 (analysis not shown). In contrast, for the intermediate times (3, 18, and 125 ms), a minimum of four bands arising from the tautomers of two species, the external aldimine with Orn or putrescine (species 1), and a quinoid species (species 2), are required to provide a good fit to the data (Figure 6 and Table 1). The spectrum of the quinoid species from this analysis is strikingly similar to species B obtained from the global kinetic deconvolution of the data (Figure 5a). At the time of maximal accumulation (18 ms) of the 445 nm band, the Schiff base species is calculated to account for 80% of the total absorbance (27 and 53% contribution for the two tautomeric bands at 420 and 328 nm, respectively) and the quinoid species is calculated to account for 20% of the total

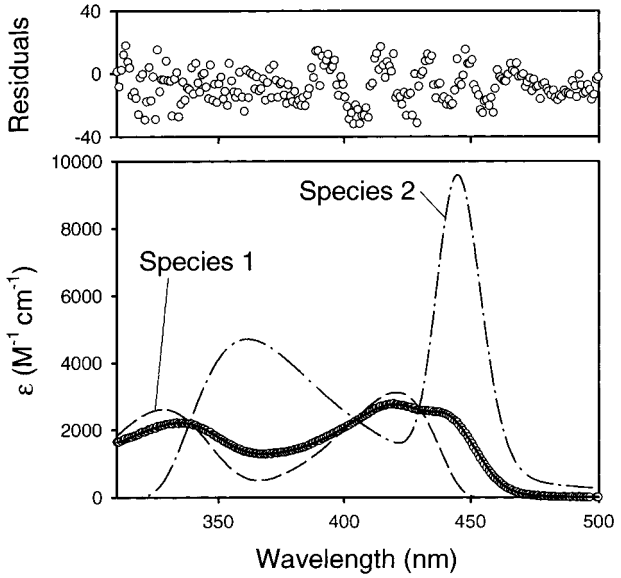

FIGURE 6: Reconstruction of the spectra of ODC reaction intermediates using log-normal distribution curves. The spectra obtained 18 ms after mixing ODC (0.16 mM) and Orn (10 mM) were analyzed according to eq 3. The data were reconstructed by the addition of four bands (Table 1) arising from the tautomers of two species. Species 1 (dashed lines) is characteristic of a Schiff base and species 2 (dot/dashed lines) is characteristic of a quinoid intermediate. The species are displayed in their observed tautomeric ratios normalized to a 1 M solution of pure species. The fit to the data (open circles) was calculated by log-normal analysis (eq 3) using 80% species 1 and 20% species 2 and is displayed as the solid line. The residual plot for the fit is displayed above the graph.

Table 1: Band Parameters from the Spectral Deconvolution of the Data Acquired 18 ms after Mixing ODC and Orn[a]

band maxima (nm)	width ($cm^{-1} \times 10^{-3}$)	skewness	A ($m \cdot mol^{-1}$) $\times 10^{-6}$	A_o ($m \cdot mol^{-1}$) $\times 10^{-6}$
445	1.0	1.0	19	439
(450−525)[a,b]	(0.9−1.6)[a]	(1.0−1.1)[a]		
420	2.5	1.8	72	265
(423−431)[c]	(3.4−3.9)[c]	(1.4−1.6)[c]		
360	4.7	0.63	50	313
(345−387)[a,d]	(1.6−3.5)[a,d]	(1.0)[a]		
328	4.4	1.4	98	186
(327−334)[c]	(3.7−5.3)[c]	(1.3−1.4)[c]		

[a] Parameters (band maxima, width, skewness, and area (A)) were calculated from the 18 ms time point spectra in Figure 4a using eq 3. Parameters in parentheses are based on published data for other PLP-dependent enzymes: refs [a]34; [b]14, 35, 40−43, 45, and 46; [c]33 and 35; [d]14. The molar areas (A_o) were derived from literature values as follows: A_o for the 445 nm band was assumed to be the same as the 470 nm quinoid from tryptophanase (*35*), A_o for the 420 and 328 nm bands were assumed to be the same as A_o's for the internal aldimine of ODC, which were calculated based upon the A_o for the ketoenamine and enoliminine tautomers of tryptophanase (*35*) and aspartate aminotransferase (*33*), and A_o for the 360 nm band was calculated from the remaining unaccounted fraction of ODC.

absorbance (16% contribution from the 360 nm band and 4% contribution from the 445 nm band).

Global Kinetic Analysis of the Reaction of ODC with Putrescine. The reaction of putrescine (10 mM) with ODC (0.16 mM) was characterized by multiwavelength stopped-flow analysis at 4 °C (Figure 4b). In contrast to the data acquired for Orn (Figure 4a), the 450 nm shoulder is absent in the reaction with putrescine. In the initial phase of this reaction, which occurs in the dead time of the mixer, there is a decrease in absorbance at 420 nm and an increase in absorbance at 335 nm. In the second phase of the reaction, complete at 18 ms, there is a small increase at 420 nm and a decrease at 335 nm. The third phase of the reaction is characterized by a larger increase at 420 nm and a decrease at 335 nm.

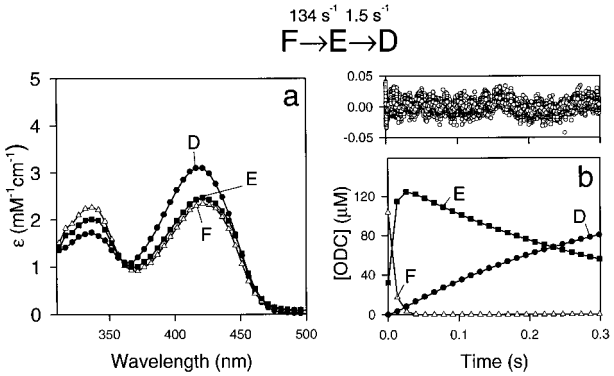

FIGURE 7: Global kinetic analysis of the mulit-wavelength stopped-flow data acquired after mixing ODC (0.16 mM) with 10 mM putrescine (representative spectra are displayed in Figure 4b). Data were fit by global kinetic analysis to the equation which describes a two-step sequential reaction model (scheme 2), with three species (D−F) interconverted by two rate constants (134 ± 6, 1.46 ± 0.05 s^{-1}, where the errors are the standard deviation of the mean for four independent determinants). The standard deviation (σ) of the absorbance for this model is 0.0012 ± 0.0002**.** The rate constants and σ represent the average of four independent experiments; the error is the standard deviation. The analysis for a representative data set is displayed. (a) The model-derived wavelength dependence of the extinction coefficients for intermediates D (●), E (■), and F (△). (b) The model-derived concentration profiles for intermediates D−F. The residuals to the fit are shown as described for Orn in Figure 5. Data points were collected at 0.84 nm intervals but are displayed at 5 nm intervals.

Scheme 2

$$F \longrightarrow E \longrightarrow D$$

Global kinetic analysis of the data acquired for the putrescine reaction suggests that they are best fit to the equation for a two-step sequential reaction (Scheme 2), where F is the initial adduct formed between ODC and putrescine, and E and D are intermediates which convert with rate constants of 134 ± 6 and 1.46 ± 0.05 s^{-1} respectively. The amplitude change associated with the conversion of species F to species E is small in comparison to the conversion of the initial spectra to species F. For this reason we considered the possibility that the data should be modeled by a single-step reaction (F → D) described by one rate constant (1.4 s^{-1}). However, the error associated with this model (σ = 0.0018 ± 0.0001) is higher than the error associated with the two-step model (σ = 0.0012 ± 0.0002), and systematic deviations were observed in the residual plots that are absent in the two-step model. Based on the two step model, the spectra for species D−F were calculated (Figure 7a,b). All three species have absorbance maxima at 335 and 420 nm, similar again to the internal aldimine. Significantly, there is no evidence for the presence of a species with spectral properties similar to species B in the Orn reaction.

Measuring the Putrescine Off Rate. The finding that DTT reacts with free ODC and is associated with a large spectral change at 420 nm was exploited as a method to determine putrescine off rates. DTT was used as a chemical trap to measure the rate of formation of free ODC upon dilution of a preformed ODC/putrescine complex. The spectral changes associated with DTT binding are much larger than the spectral changes associated with putrescine; thus, all spectral

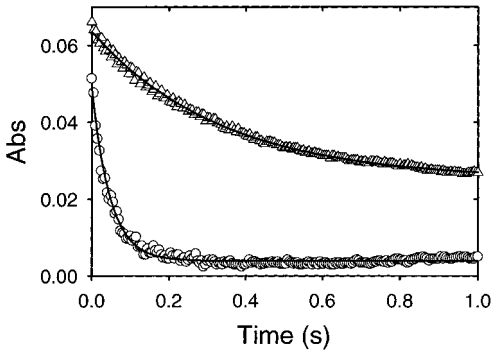

FIGURE 8: Measurment of the putrescine off rate by trapping free ODC with DTT: (○) absorbance change observed upon mixing ODC (0.03 mM) and DTT (0.2 M); (△) absorbance change upon 10-fold dilution of an ODC (0.30 mM)/putrescine (4 mM) mixture into DTT (0.2 M) buffer solution. The solid lines represent a single-exponential fit to eq 1, (○) $k_{DTTon} = 23.4 \pm 0.4\ s^{-1}$ and (△) $k_{trap} = 3.1 \pm 0.2\ s^{-1}$. The rate constants are the average of four independent experiments; the error is the standard deviation. The analysis for a representative data set is displayed. Data were collected at 4 °C.

changes observed at 420 nm in the presence of DTT are associated with the DTT reaction. Since the DTT on rate is fast relative to the putrescine off rates, the kinetics of the spectral changes upon dilution of the ODC/putrescine complex into DTT are dominated by the putrescine off rate.

Putrescine (4 mM) was preincubated with ODC at concentrations above the K_I (0.6 mM (*5*)) such that all enzyme was complexed to putrescine. The ODC/putrescine complex was diluted 10-fold into DTT to below the K_I (Figure 8), and the spectral changes at 420 nm were recorded. As a control DTT was reacted with free ODC. The data were fit to a single exponential (eq 1); k_{obs} for DTT (200 mM) and ODC alone is $23.4 \pm 0.4\ s^{-1}$ (k_{DTTon}) and k_{obs} for the decay of the ODC/putrescine complex is $3.1 \pm 0.2\ s^{-1}$ (k_{trap}). Halving of the DTT concentration (100 mM) decreases the k_{DTTon} ($11.0 \pm 0.6\ s^{-1}$) for the reaction of DTT in the absence of putrescine but does not significantly change k_{trap} ($2.3 \pm 0.3\ s^{-1}$), demonstrating that the observed rate constants in the latter case are dominated by the putrescine off rates.

DISCUSSION

UV−visible stopped-flow analysis of reaction intermediates has not been extensively utilized to study PLP-dependent decarboxylases despite the wealth of data acquired for other PLP enzyme-catalyzed reactions (e.g., aspartate aminotransferase (*16*−*18*), tryptophan synthase (*39*), and tryptophanase (*40*)). In these well described examples, the enzymes typically utilize multiple substrates, and therefore, partial reactions can be followed and spectrally distinct species are observed (e.g., the formation of PMP from PLP in the aspartate aminotransferase half-reaction is readily monitored). In contrast, decarboxylases utilize a single substrate; thus, no part of the reaction can be isolated to aid in the analysis. In the reaction of ODC with Orn, single-wavelength data analysis provided kinetic information, but analysis of the substrate dependence of these data to obtain mechanistic information was complicated by two factors. First, because of the high enzyme concentrations required to observe the reaction, the rates may be effected by stoichiometric binding for substrate concentrations below 1 mM. Second, multiple species and tautomers of PLP contribute to the observed spectra at all wavelengths, making it difficult to determine whether single or multiple processes are contributing to each k_{obs}. Additionally, the single-wavelength data analysis cannot resolve the spectra of intermediates with features distinct from the dominant Schiff base species; thus, little mechanistic information is obtained. However, the powerful deconvolution features of global kinetic analysis of the multiwavelength data allow a unique spectral species to be identified in the ODC reaction. This analysis, combined with the extensive literature describing the absorbance spectra of PLP derivatives, species, and tautomers (see Table 1), has allowed us to define a minimal mechanism for the decarboxylation of Orn by ODC.

The absorbance spectra of species A and D (Figure 5a) formed in the reaction of ODC with Orn are consistent with a Schiff base species (Table 1) between PLP and substrate (species A) or product (species D). In contrast, species B has unique absorbance spectra with the predominant maxima occurring at 350 and 450 nm. These absorbance maxima are similar to the absorbance maxima reported for the two tautomers of the quinoid intermediate observed in glutamate decarboxylase (*14*), providing strong support for the assignment of species B as the quinoid intermediate in the ODC reaction. Further, the quinoid intermediates reported for many other PLP enzymes are also characterized by a species with an absorbance maxima between 460 and 525 nm (e.g., 480−525 nm for aspartate aminotransferase (*34*, *41*, *42*), 460−476 nm for tryptophan synthase (*43*), and 500 nm for tryptophanase (*40*)). Interestingly, the ODC and glutamate decarboxylase quinoid is characterized by a shorter wavelength species than observed for these other PLP-dependent enzymes. However, these enzymes remove the α-proton to form the quinoid species and leave the CO_2 in the PLP plane, allowing for greater conjugation. In contrast, the decarboxylases remove CO_2, which would result in a blue shift of the wavelength maxima of the quinoid species (*44*).

The assignment of species B as the quinoid intermediate is further supported by spectral deconvolution of the data (Table 1, Figure 6). The spectra at 18 ms after mixing ODC with Orn can be reconstructed by adding together bands describing two species, the two tautomers of a Schiff base species plus the two tautomers of a quinoid species. The spectrum of the reconstructed quinoid species obtained by this method is very similar to the spectrum of species B obtained by global kinetic analysis of the data, though the 350 nm peak is predicted by the spectral deconvolution to be less prominent and red shifted compared to species B. In addition to the absorbance maxima, the calculated parameters (ω_1, ρ_1) that define the spectral bands are similar to those reported for the Schiff base and quinoid species in other PLP-dependent enzymes (Table 1). Thus, both methods of analysis predict that similar intermediates are formed during the reaction of ODC with Orn. It is still feasible that an additional unidentified spectral species may be formed which neither of the methods is able to resolve. For example, the Schiff base species in which the imine nitrogen is unprotonated could be forming during the course of the reaction. This species has an absorbance maxima of 360 nm (*17*, *34*) and would have a particularly strong effect on the analysis of the 350 nm species. However, because the 350 and 450 nm peaks build up with the same kinetic profile during the reaction, we favor the hypotheses that they arise predominately from tautomers of a single species (the quinoid).

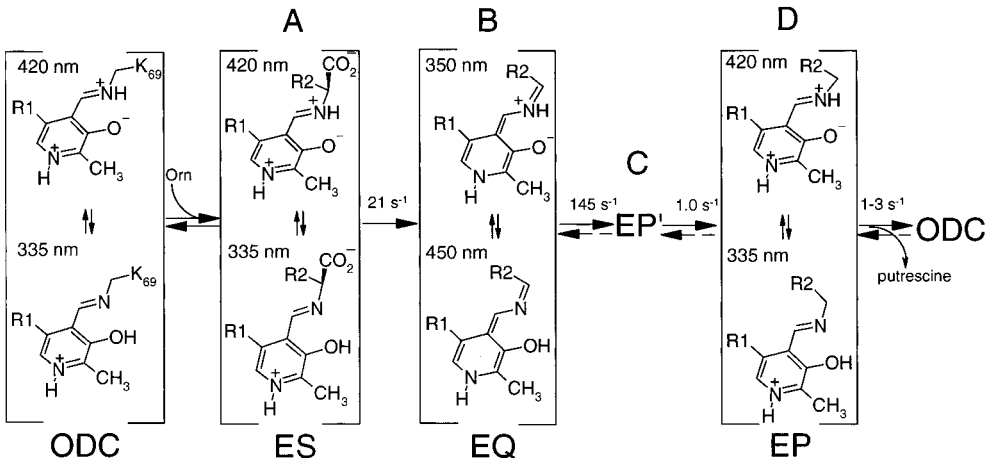

FIGURE 9: Model for the mechanism of decarboxylation of Orn by ODC. The wavelength maxima are based upon the results reported in Figure 5a. The assignment of absorbance bands to the individual tautomers for the Schiff base species A and D (*32*, *44*) and for the quinoid species B (*34*, *41*) is based on the cited literature.

Nonetheless, we cannot rule out the possibility that, at least in part, they arise from separate species which are formed with similar rate constants (e.g., the 350 nm peak could represent the Schiff base species in which the imine nitrogen is unprotonated and the 450 nm peak the quinoid).

Studies on model compounds by Metzler and co-workers suggest that the 350 nm band of the quinoid species arises from the tautomer in which the proton is on the imine nitrogen, while the 450 nm band arises from the tautomer protonated on the 3′-hydroxyl (Figure 9 (*34*, *41*)). Our data suggest that the 350 nm band is the predominate quinoid tautomer in ODC. A similar result has been reported for glutamate decarboxylase (*14*), while the longer wavelength band is the predominate tautomer in the aspartate aminotransferase quinoid (*42*). Molecular orbital calculations suggest that the tautomer that is protonated on the imine nitrogen has a greater propensity to be protonated on C_α than at C4′, while the tautomer that is protonated on the 3′-hydroxyl has the opposite preference. Assuming that the analysis of model compounds accurately reflects the properties of PLP when bound to an enzyme active site, these observations suggest that the tautomeric ratio of the quinoid species is involved in controlling the reaction specificity. For the decarboxylases, protonation at C4′ leads to abortive deamination while protonation at C_α leads to correct product formation. Thus, by promoting the 350 nm quinoid tautomer over the 450 nm structure, the decarboxylases direct the reaction toward protonation at C_α. In contrast, the tautomeric ratios are reversed in the aspartate aminotransferase reaction where protonation at C4′ is required to form the correct products of the first half-reaction.

The identification of species B as the quinoid intermediate allows an overall reaction mechanism for catalysis by ODC to be constructed (Figure 9). Because the quinoid species is expected to be generated only upon decarboxylation, the conversion of species A to species B most likely represents decarboxylation. Thus, the data suggest that the reaction proceeds via formation of a Schiff base intermediate (species A) during the dead time of the stopped-flow instrument, followed by formation of a quinoid intermediate with a rate constant of 21 s^{-1}. The quinoid intermediate decays in two steps to a Schiff base with putrescine (species D). The nature of the chemical events that occur in these two steps cannot be definitively determined from the current data. The spectral characteristics of species C are predominately that of a Schiff base; however, this species has an altered tautomeric ratio when compared to a typical Schiff base with PLP. Protonation of the C_α carbon is required to form putrescine. The quinoid could be protonated either directly at C_α or it could initially be protonated at C4′ and then form putrescine through a 1,3-prototropic shift (Figure 1). However, there is no evidence for an increase in 330 nm absorbance, which would be expected if protonation occurred at C4′. Thus, the quinoid is likely to be protonated directly at the C_α carbon to form a Schiff base with putrescine in the first of the two steps (k_2 = 145 s^{-1}); species C then decays in a slow step (1.0 s^{-1}) to species D. Two plausible explanations as to the chemical nature of this slow step are either regeneration of the proton donor or a conformational change.

Putrescine reacts with the enzyme via two steps to form a species with characteristic Schiff base spectral properties equivalent to species D in the reaction with Orn (i.e., the external aldimine with putrescine). The chemical nature of the remaining species (E and F, designated below as E/F for simplicity) is not understood; however, both a Michaelis complex and a gem diamine intermediate are expected to precede Schiff base formation. Species E/F also has Schiff base spectral characteristics; however, the data suggest that the only common intermediate between the reaction of ODC with Orn and the reaction of ODC with putrescine is species D. The amplitude change upon converting species E to D for the reaction with putrescine is opposite to that expected if this were the same step as the C to D conversion observed in the reaction with Orn. Thus, the combined Orn and putrescine data suggest that the minimal reaction mechanism which can describe the ODC reaction is ODC + S ⇔ A → B → C → D → E/F ⇔ ODC + P, where decarboxylation (A → B) is irreversible but the other steps are assumed to be reversible (Figure 9). Notably, the rate of decarboxylation (k_1 = 21 s^{-1}) is fast relative to the slow steps in the reaction that are associated with the decay of species C to species D (k_3 = 1 s^{-1}) and with product release (e.g., the multistep decay of species D to free enzyme and product that occurs with a rate constant no greater than 1.5 s^{-1}). In comparison to k_{cat} (0.5 s^{-1}) for the steady-state reaction, these data indicate that product release is a rate-determining step. This

hypothesis is further supported by the independent measurement of the putrescine off rates ($k_{off} = 3\ s^{-1}$) utilizing the DTT trap protocol.

In conclusion, the mechanism of ODC has been demonstrated to proceed via a quinoid intermediate. Interestingly, decarboxylation is not rate limiting, being 40 times faster than k_{cat}, and instead the rate of product release ($1-3\ s^{-1}$) is identified as a rate-limiting step. These experiments provide the first detailed mechanistic analysis of a PLP-dependent decarboxylase, and they set the stage for more detailed analysis of the roles of active site residues in ODC-catalyzed decarboxylation.

ACKNOWLEDGMENT

We thank V. Davidson, P. Thomas, and Molecular Kinetics (Y. Van and K. Dunker) for generously allowing us access to their stopped-flow equipment, G. Ford for performing the molecular orbital calculations, and B. Peterson for helpful discussions.

REFERENCES

1. Pegg, A. E., and Williams-Ashman, H. G. (1968) *Biochem. J. 108*, 533−539.
2. Marton, L. J., and Pegg, A. E. (1995) *Annu. Rev. Pharmacol. Toxicol. 35*, 55−91.
3. Wang, C. C. (1995) *Annu. Rev. Pharmacol. Toxicol. 35*, 93−127.
4. McCann, P. P., and Pegg, A. E. (1992) *Pharm. and Therap. 54*, 195−215.
5. Osterman, A. L., Grishin, N. V., Kinch, L. N., and Phillips, M. A. (1994) *Biochemistry 33*, 13662−13667.
6. Tobias, K. E., and Kahana, C. (1993) *Biochemistry 32*, 5842−5847.
7. Coleman, C. S., Stanley, B. A., Viswanath, R., and Pegg, A. E. (1994) *J. Biol. Chem. 269*, 3155−3158.
8. Grishin, N. V., Phillips, M. A., and Goldsmith, E. J. (1995) *Protein Sci. 4*, 1291−1304.
9. Shaw, J. P., Petsko, G. A., and Ringe, D. (1997) *Biochemistry 36*, 1329−1342.
10. Poulin, R., Lu, L., Ackerman, B., Bey, P., and Pegg, A. E. (1992) *J. Biol. Chem. 267*, 150-158.
11. Coleman, C. S., Stanley, B. A., and Pegg, A. E. (1993) *J. Biol. Chem. 268*, 24572−24579.
12. Osterman, A. L., Kinch, L. N., Grishin, N. V., and Phillips, M. A. (1995) *J. Biol. Chem. 270*, 11797−11802.
13. Osterman, A. L., Brooks, H. B., Rizo, J., and Phillips, M. A. (1997) *Biochemistry 36*, 4558−4567.
14. Sukhareva, B.S. (1986) in *Vitamin B6, pyridoxal phosphate* (Dolphin, D., Poulson, R., and Avramovic, O., Eds.) pp 325−353, John Wiley and Sons Inc., New York.
15. Drewe, W. F., Jr., Koerber, S. C., and Dunn, M. F. (1989) *Biochimie 71*, 509−519.
16. Julin, D. A., and Kirsch, J. F. (1989) *Biochemistry 28*, 3825−3833.
17. Kirsch, J. F., Eichele, G., Ford, G. C., Vincent, M. G., and Jansonius, J. N. (1984) *J. Mol. Biol. 174*, 497−525.
18. Toney, M. D., and Kirsch, J. F. (1993) *Biochemistry 32*, 1471−1479.
19. Akhtar, M., Stevenson, D. E., and Gani, D. (1990) *Biochemistry 29*, 7648−7660.
20. Phillips, M. A., Coffino, P., and Wang, C. C. (1987) *J. Biol. Chem. 262*, 8721−8727.
21. Phillips, M. A., Coffino, P., and Wang, C. C. (1988) *J. Biol. Chem. 263*, 17933−17941.
22. Coligan, J. E., Dunn, B. M., Ploegh, H. L, Speicher, D. W., and Wingfield, P. T. (1995) in *Current protocols in protein science* (Coligan, J. E., Dunn, B. M., Ploegh, L. P., Speicher, D. W., and Wingfield, P. T., Eds.) 1995 John Wiley & Sons Inc., Brooklyn, NY.
23. Brooks, H. B., and Phillips, M. A. (1996) *Anal. Biochem. 238*, 191−194.
24. Segel, I. H. (1975) in *Enzyme kinetics, behavior and analysis of rapid equilibrium and steady-state enzyme systems* (Segel, I. H., Ed.) John Wiley & Sons, Inc., New York.
25. Malinowski, E. R. (1991) in *Factor analysis in chemistry*. (Malinowski, E. R., Ed.) John Wiley & Sons Inc., New York.
26. Stultz, L. K., Binstead, R. A., Reynolds, M. S., and Meyer, T. J. (1995) *J. Am. Chem. Soc. 117*, 2520−2532.
27. Strickland, S., Palmer, G., and Massey, V. (1975) *J. Biol. Chem. 250*, 4048−4052.
28. Hiromi, K. (1979) *Kinetics of Fast Enzyme Reactions: Theory and Practice* (Hiromi, K., Ed.) Halsted Press, New York.
29. Siano, D. B., and Metzler, D. E. (1969) *J. Chem. Phys. 51*, 1856−1861.
30. Harris, C. M., Johnson, R. J., and Metzler, D. E. (1976) *Biochim. Biophys. Acta 421*, 181−194.
31. Metzler, D. E., Harris, C. M., Johnson, R. J., Saino, D. B., and Thomson, J. A. (1973) *Biochemistry 12*, 5377−5392.
32. Metzler, C. M., Cahill, A., and Metzler, D. E. (1980) *J. Am. Chem. Soc. 102*, 6075−6082.
33. Metzler, C. M., and Metzler, D. E. (1987) *Anal. Biochem. 166*, 313−327.
34. Metzler, C. M., Harris, A. G., and Metzler, D. E. (1988) *Biochemistry 27*, 4923−4933.
35. Metzler, C. M., Viswanath, R., and Metzler, D. E. (1991) *J. Biol. Chem. 266*, 9374−9381.
36. Dewar, M. J. S., Zoebisch, E. G., Healy, E. F., and Stewart, J. J. P. (1985) *J. Am. Chem. Soc. 107*, 3901−3909.
37. Buell, M. V., and Hansen, R. E. (1960) *J. Am. Chem. Soc. 82*, 6042−6049.
38. Seely, J. E., Poso, H., and Pegg, A. E. (1983) *Methods Enzymol. 94*,
39. Brzovic, P. S., and Dunn, M. F. (1995) *Methods Enzymol. 246*, 168−201.
40. Lee, M., and Phillips, R. S. (1995) *Bioorg. Med. Chem. 3*, 195−205.
41. Chen, V. J., Metzler, D. E., and Jenkins, W. T. (1987) *J. Biol. Chem. 262*, 14422−14427.
42. Toney, M. D., and Kirsch, J. F. (1991) *J. Biol. Chem. 266*, 23900−23903.
43. Drewe, W. F., Jr., and Dunn, M F. (1986) *Biochemistry 25*, 2494−2501.
44. Morozov, Y. V. (1986) in *Vitamin B6 pyridoxal phosphate* (Dolphin, D., Poulson, R., and Avramovic, O., Eds.) pp 325−353, John Wiley & Sons, Inc., New York.
45. del Pozo, A. M., Pospischil, M. A., Ueno, H., Manning, J. M., Tanizawa, K., Nishimura, K., Soda, K., Ringe, D., Stoddard, B., and Petsko, G. A. (1989) *Biochemistry 28*, 8798−8803.
46. Hansen, J., and Davis, L. (1979) *Biochim. Biophys. Acta. 568*, 321−30.
47. Brzovic, P. S., Hyde, C. C., Miles, E. W., and Dunn, M. F. (1993) *Biochemistry 32*, 10404−10413.
48. Drewe, W. F., Jr., and Dunn, M. F. (1985) *Biochemistry 24*, 3977−3987.
49. O'Leary, M. H. (1971) *Biochim. Biophys. Acta. 242*, 484−492.
50. Hidalgo, C., Seville, J. M., Pineda, T., and Blazquez, M. (1994) *J. Phys. Org. Chem. 7*, 227−233.

BI971652B